

# Flow Characteristics around Rectangular Obstacles with the Varying Direction of Obstacles

Hee-Chang Lim

**Abstract**—The study aims to understand the surface pressure distribution around the bodies such as the suction pressure in the leading edge on the top and side-face when the aspect ratio of bodies and the wind direction are changed, respectively. We carried out the wind tunnel measurement and numerical simulation around a series of rectangular bodies ( $40^d \times 80^w \times 80^h$ ,  $80^d \times 80^w \times 80^h$ ,  $160^d \times 80^w \times 80^h$ ,  $80^d \times 40^w \times 80^h$  and  $80^d \times 160^w \times 80^h$  in  $\text{mm}^3$ ) placed in a deep turbulent boundary layer. Based on a modern numerical platform, the Navier-Stokes equation with the typical 2-equation ( $k-\epsilon$  model) and the DES (Detached Eddy Simulation) turbulence model has been calculated, and they are both compared with the measurement data. Regarding the turbulence model, the DES model makes a better prediction comparing with the  $k-\epsilon$  model, especially when calculating the separated turbulent flow around a bluff body with sharp edged corner. In order to observe the effect of wind direction on the pressure variation around the cube (e.g.,  $80^d \times 80^w \times 80^h$  in mm), it rotates at  $0^\circ$ ,  $10^\circ$ ,  $20^\circ$ ,  $30^\circ$ , and  $45^\circ$ , which stands for the salient wind directions in the tunnel. The result shows that the surface pressure variation is highly dependent upon the approaching wind direction, especially on the top and the side-face of the cube. In addition, the transverse width has a substantial effect on the variation of surface pressure around the bodies, while the longitudinal length has little or no influence.

**Keywords**—Rectangular bodies, wind direction, aspect ratio, surface pressure distribution, wind-tunnel measurement,  $k-\epsilon$  model, DES model, CFD.

## I. INTRODUCTION

REGARDING the flow around buildings of all kinds, numerous data have been generated and comparisons have even been made between experimental and numerical data. One often-cited paper is the wind-tunnel study of Castro and Robins [1], which measured the flow around surface-mounted cubes. According to Tieleman and Akins [2], the body geometry (i.e. the aspect ratio of the body) has an effect on the variation of the surface pressure. In addition to the research on changes in aspect ratios, the effects of wind direction have also been studied by many researchers (i.e. Richards et al. [3]). As regards the CFD techniques, the accuracy of the numerical calculation was highly dependent upon the choice of turbulence model. In more recent times, the DES model shows a high potential in practical applications (see e.g. Jochen and Dominic [4]).

The emphasis of this paper is on the flow characteristics around rectangular bodies with various aspect ratios and wind directions. The standard  $k-\epsilon$  and the DES model were used, and the results were ultimately compared with the

experimental data (i.e. the wind tunnel and the existing field data).

## II. EXPERIMENTAL TECHNIQUES

Fig. 1 illustrates the detailed set-up inside the boundary layer wind tunnel, showing a grid, a tripping fence, roughness, and a cube model. The wind tunnel is suitable for generating an artificial boundary layer and is also equipped with a modern hot-wire anemometer (IFA100), a multi-channel pressure scanning system, and a PIV system for optical measurement of the airflow. Smooth-surface rectangular bodies used in the tunnel were made of plexiglass and consisted of five bodies:  $80^{long} \times 80^{wide} \times 80^{high}$  (h) in mm for  $1 \times 1$ ,  $40^l \times 80^w \times 80^h$  for  $2 \times 1s$ ,  $160^l \times 80^w \times 80^h$  for  $1 \times 2$ ,  $80^l \times 40^w \times 80^h$  for  $1 \times 2s$  and  $80^l \times 160^w \times 80^h$  for  $2 \times 1$ .

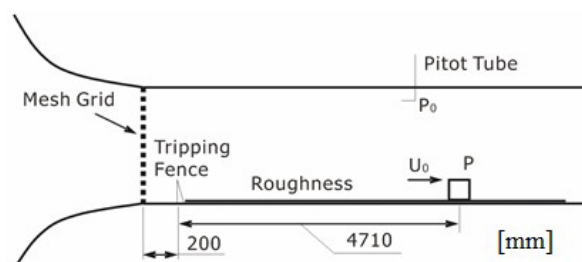


Fig. 1 The  $0.6 \text{ m} \times 0.72 \text{ m} \times 6 \text{ m}$  section of the wind tunnel test

## III. COMPUTATIONAL TECHNIQUES

A schematic diagram of the numerical channel with a wall-mounted bluff body is shown in Fig. 2 (a). The domain size and the boundary conditions can be seen easily from this figure. In the case in which the wind direction was changed (symbolised as  $\phi$ , which stands for  $0^\circ$ ,  $10^\circ$ ,  $20^\circ$ ,  $30^\circ$ ,  $45^\circ$ , respectively), a schematic model was shown in Fig. 2 (b). In terms of the mesh size used to resolve the small-scale turbulent flow, a fine mesh resolution near the (model) wall was used, with the first grid spacing near the wall was  $0.025h$  to ensure that wall  $y^+$  was acceptable. When the aspect ratio of the models varies, the computational domain and the number of grids must be reconstructed. The present numerical simulation was carried out according to the experimental study. Fig. 3 compares the profiles of the inlet mean-velocity (a) and turbulence intensity (b) in the streamwise components. In addition, the typical longitudinal-velocity spectra,  $E_u(f)$ , obtained at  $z = h$  in the channel flow was presented in Fig. 3 (c), which are compared with the standard spectra ESDU.

Heechang Lim is with the Pusan National University, Korea, Republic Of (e-mail: helim@pusan.ac.kr).

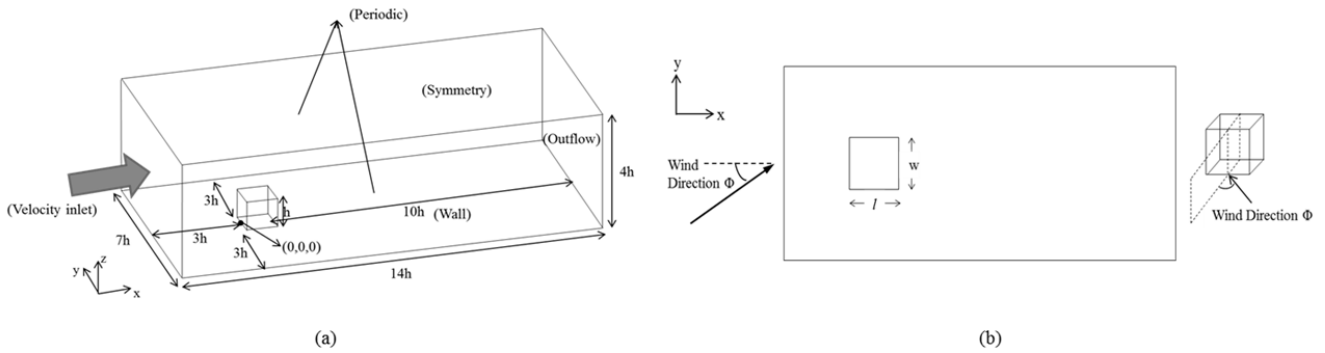


Fig. 2 Schematic diagram of the numerical channel

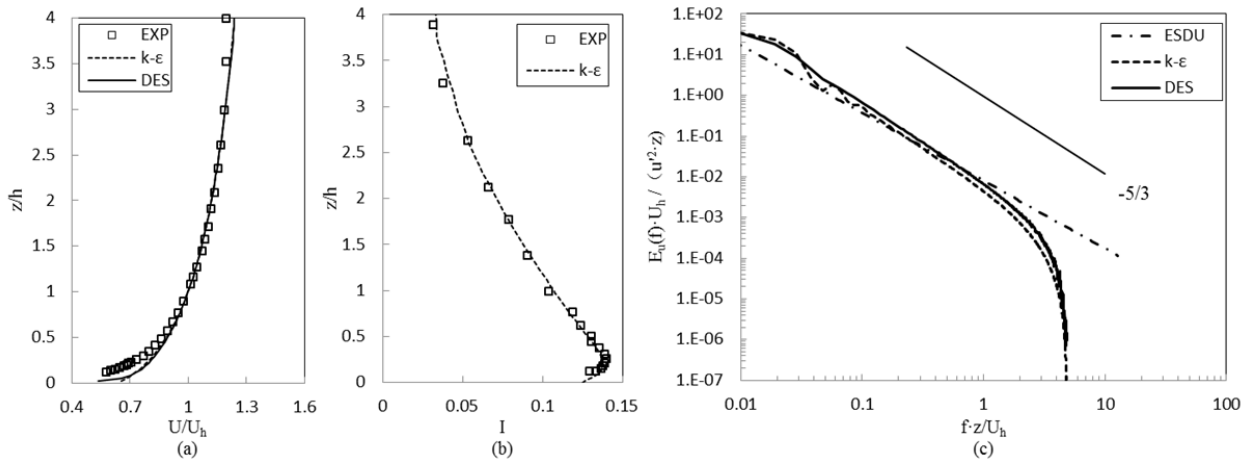


Fig. 3 (a) The inlet mean-velocity; (b) Turbulence intensity; (c) Longitudinal-velocity spectra

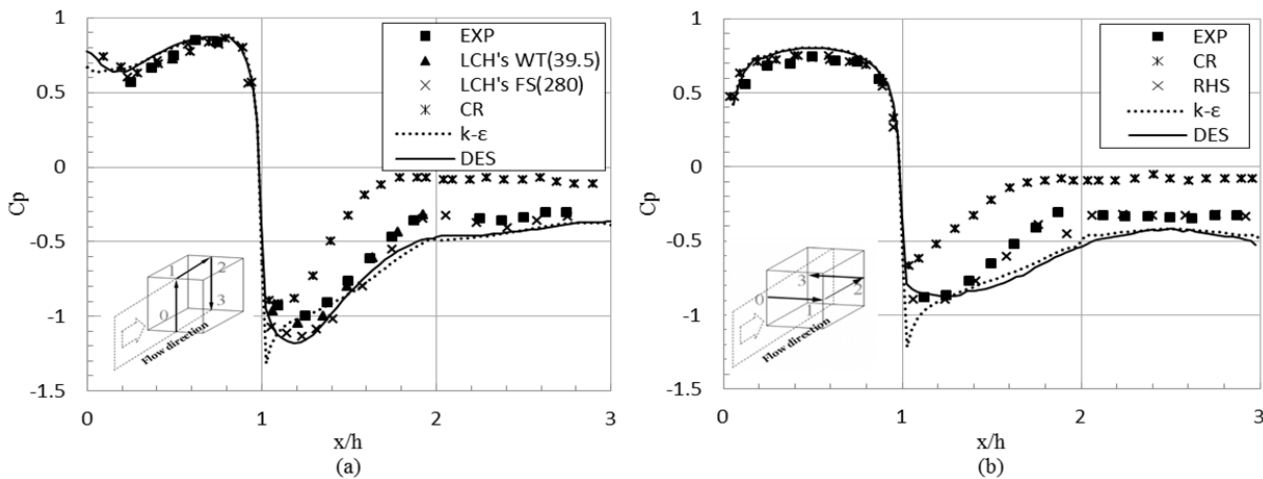


Fig. 4 Mean surface static pressure coefficient: (a) along the centerline; (b) at the mid-height

#### IV. RESULTS AND DISCUSSION

##### A. Surface Pressure Distribution - A Cubical Model (1 × 1)

Fig. 4 compares the numerical and experimental results for the variations of the mean static pressure coefficient  $C_p = (p - p_r) / (0.5\rho U_h^2)$ . Both the results along the centreline (Fig. 4 (a)) and at the mid height (Fig. 4 (b)) have an expected shape. In addition, the CFD results agree well with the wind tunnel and the existing field data (e.g. Lim et al. [5]), furthermore the

DES model seems to offer better performance than the k- $\epsilon$  model. However, there still have some scatters between each result which may be caused by the different turbulence levels.

##### B. Surface Pressure Distribution - Models with Aspect Ratio

As the DES model performed better than the k- $\epsilon$  model, we compared the numerical DES data with the experimental wind-tunnel data with various aspect ratios in this chapter.

Figs. 5 and 6 separately present the mean surface static pressure profiles along the centerline and at the mid-height with changes in the transverse width. Note that (a) shows the experiment data, (b) shows the DES data, while the schematics of the models are showed on the right side. In addition, the subsequent figures are arranged in the same manner as in Fig. 5. The immediate implication of Fig. 5 is that the wider the shape of the body, the stronger the surface suction pressure on the top surface. Fig. 6 demonstrates that, with an increase in the horizontal width, there is a concurrent suction pressure

drop on the side face.

Figs. 7 and 8 show the mean surface static pressure profiles along the centerline (top face) and at the mid-height (side face) of the models with changes in the longitudinal length. In the figures, the pressure profiles seem to show a similar trend, and we would note that the overall distribution of the surface pressure is in good agreement. We may thus draw the conclusion that the longitudinal length of the body has little or no influence on the surface pressure around rectangular bodies.

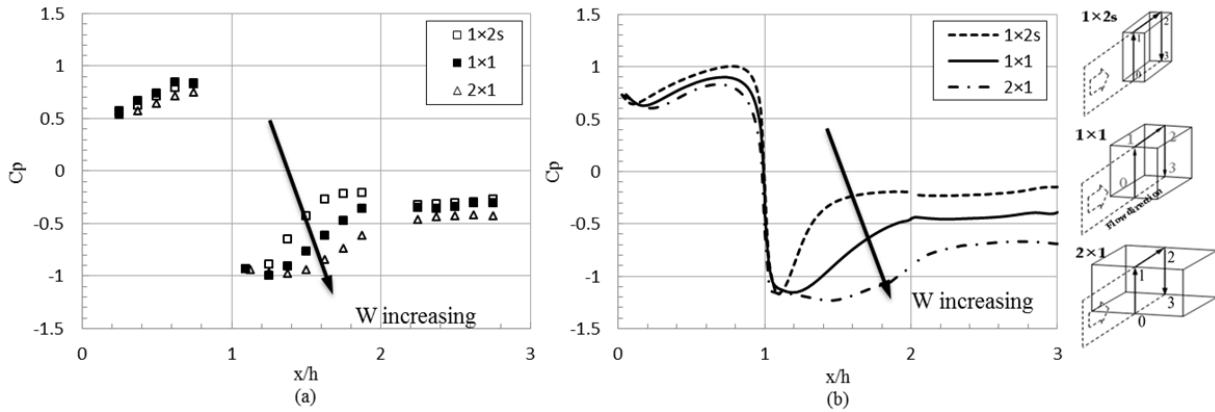


Fig. 5 Mean surface static pressure coefficient along the centerline with changing transverse width

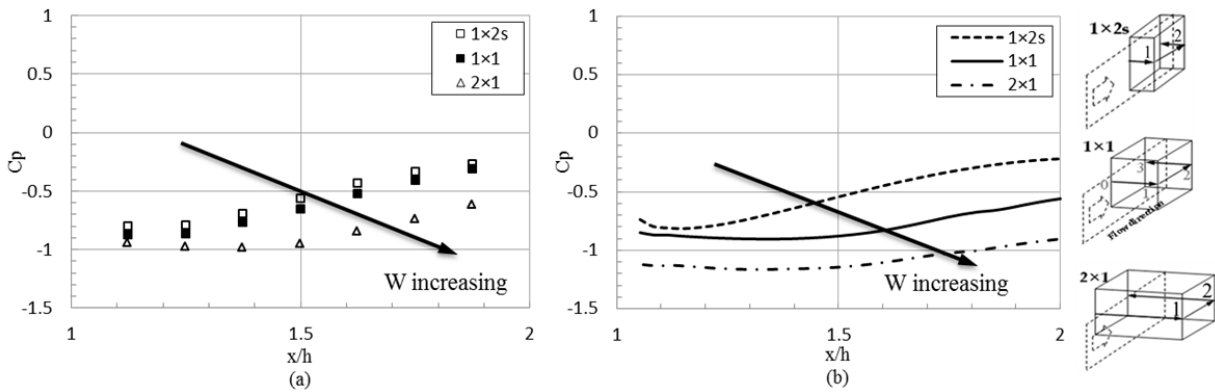


Fig. 6 Mean surface static pressure coefficient at the mid-height with changing transverse width

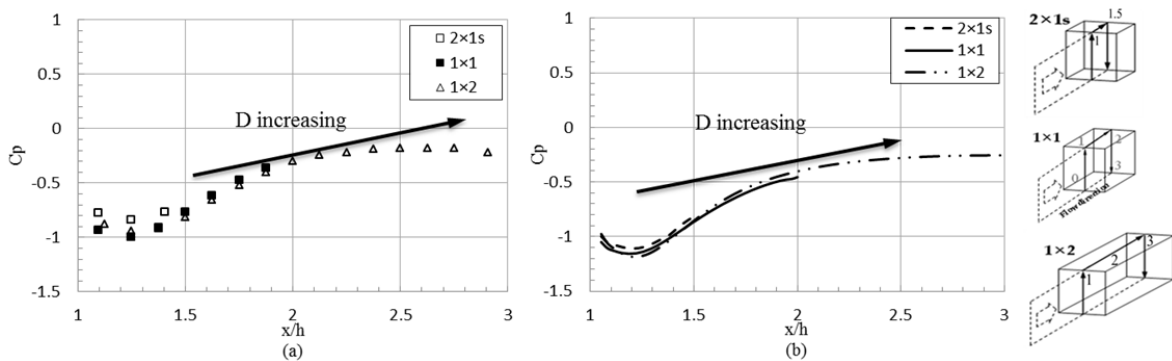


Fig. 7 Mean surface static pressure coefficient along the centerline with changing longitudinal length

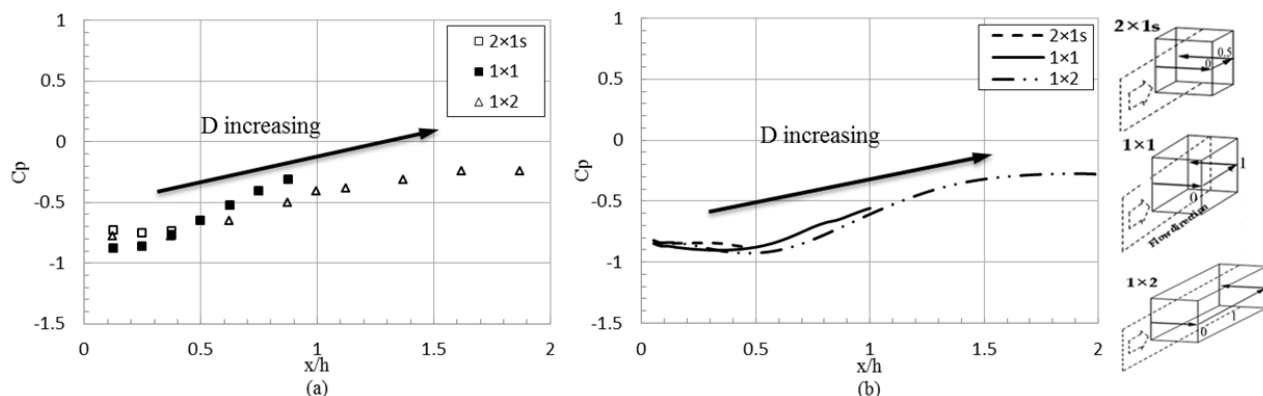


Fig. 8 Mean surface static pressure coefficient at the mid-height with changing longitudinal length

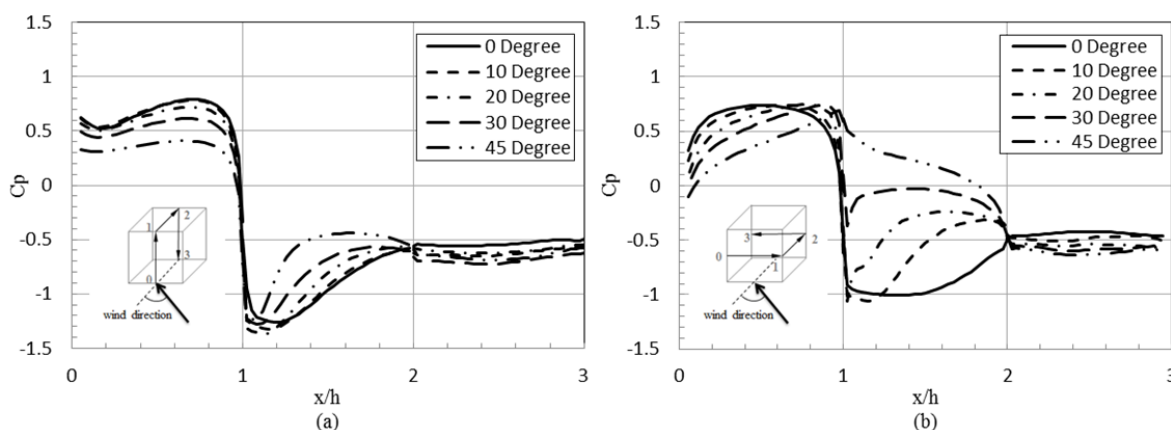


Fig. 9 Mean surface static pressure coefficient with different wind directions: (a) along the centerline; (b) at the mid-height of the cube

### C. Surface Pressure Distribution - Models with Different Wind Direction

The DES model results of the effect of wind direction on the pressure variations around the cube are shown in Fig. 9, in which (a) presents the mean static pressure coefficient along the centreline, (b) presents the one at the mid height. Both the figures are generally in good agreement with the earlier data of Richards et al. [3]. In spite of the different wind directions, the profiles have the same expected shape as before. It can also be seen that the surface pressures are highly sensitive to the wind direction. Sometimes, it can even change the pressure coefficient from a negative to a positive value.

### V. CONCLUDING REMARKS

Although more data are necessary to get definitive conclusions, this study contributes the following findings:

- (1) The CFD results are in overall agreement with the experimental results, including the existing data, though there still appears to be a small discrepancy.
- (2) The calculations performed using the DES model seem to be better than those performed with the  $k-\epsilon$  model when simulating the wind flow around a variety of bluff bodies.
- (3) When the wind direction toward a bluff body changes, the variation of the surface pressure is highly sensitive to the wind direction, especially the top face and the side face of a cubical body. Sometimes, it can even change the

pressure coefficient from a negative to a positive value.

### ACKNOWLEDGMENT

This work was supported by "Human Resources Program in Energy Technology" of the Korea Institute of Energy Technology Evaluation and Planning (KETEP), granted financial resource from the Ministry of Trade, Industry & Energy, Republic of Korea (No. 20164030201230). In addition, this work was supported by the National Research Foundation of Korea (NRF) grant funded by the Korea government (MSIP) (No. 2016R1A2B1013820).

### REFERENCES

- [1] Castro I. P. & Robins A. G. (1977). "The flow around a surface mounted cube in uniform and turbulent streams", *J. Fluid Mech.* 79, 307-335.
- [2] Tieleman H. W. & Akins R. E. (1996). "The effect of incident turbulence on the surface pressures of surface-mounted prisms", *J. Fluids and Structures.* 10, 367-393.
- [3] Richards P. J., Hoxey R. P., Connell B. D. & Lander D. P. (2007). "Wind-tunnel modelling of the Silsoe cube", *J. Wind Eng. Ind. Aero.* 95, 1384-1399.
- [4] Jochen F. & Dominic V. T. (2008). "Hybrid LES/RANS methods for the simulation of turbulent flows", *J. Progress in Aerospace Sciences*, 44(5), 349-377.
- [5] Lim H. C., Castro I. P. & Hoxey R. P. (2007). "Bluff bodies in deep turbulent boundary layers: Reynolds-number issues", *J. Fluid Mech.* 571, 97-118.